Ocean Engineering 167 (2018) 369–379

Contents lists available at ScienceDirect

Ocean Engineering

journal homepage: www.elsevier.com/locate/oceaneng

Energy balance analysis of model-scale vessel with open and ducted propeller configuration

Jennie Andersson[a,*], Arash Eslamdoost[a], Marko Vikström[b], Rickard E. Bensow[a]

[a] Chalmers University of Technology, Department of Mechanics and Maritime Sciences, 412 96, Göteborg, Sweden
[b] Rolls-Royce Hydrodynamic Research Centre, Rolls-Royce AB, Kristinehamn, Sweden

ARTICLE INFO

Keywords:
Hull-propulsion system interaction
RANS
Energy balance
Hydrodynamic losses
Ducted propeller

ABSTRACT

This paper focuses on performance analysis of a model scale vessel equipped with an open versus a ducted propeller in self-propulsion using a control volume analysis of energy, applied on Computational Fluid Dynamics (CFD) results. An energy balance analysis decompose the delivered power for each system into internal and turbulent kinetic energy fluxes, i.e. viscous losses, transverse kinetic energy losses, and pressure work and axial kinetic energy fluxes. Such a decomposition can facilitate understanding of system performance and pinpoint enhancement possibilities. For this specific case it is shown that the much higher required power for the ducted propeller configuration to the largest extent is due to higher viscous losses, caused by mainly propeller duct and different rudder configuration. The energy balance analysis is a post-processing tool with the only additional requirement of solving the energy equation, which can be employed with any CFD-code based on commonly available variables.

1. Introduction

The interaction effects between hull and propulsion system are most commonly described using a well-established terminology, including thrust deduction, wake fraction, propulsive efficiency etc. However this decomposition has its primary origin in the experimental procedures used to establish ship scale performance rather than from principles of hydrodynamics. This can imply limitations in design and optimization of hull and propulsion system, as the interaction thus may not be correctly represented. We believe that the reliability and capacity of modern Computational Fluid Dynamics (CFD) has reached a high level of maturity which can be used to extract detailed data of the flow around vessels and propulsion units.

In a previous paper (Andersson et al., 2018) an alternative approach to study the interaction effects between hull and propulsion system, based on control volume analysis of energy was outlined and applied on a propeller operating in open water. This method implies that the hydrodynamic losses associated with a high and/or uneven acceleration of the flow, slipstream rotation and viscous losses can be tracked. Quantification of the viscous losses is made possible through solving the energy equation for the flow around the vessel. A similar method aimed for marine applications have earlier been presented by van Terwisga (2013). He suggested an energy balance over a control volume enclosing the entire vessel including propulsion unit. However, through the assumption of a uniform control volume inflow, the evaluation of the fluxes were limited to the control volume downstream boundary. The method was not demonstrated in practice. More recently, Schuiling and van Terwisga (2016) suggested a methodology for performing an energy analysis based on evaluation of the energy equation over a control volume, and applied it on a propeller operating in open water. The viscous losses were obtained through volume integrals of the dissipation terms. Thus, the numerical dissipation, which cannot be evaluated from CFD, has to be obtained indirectly from the difference between delivered power, obtained from forces acting on the propeller, and the other energy components.

Interaction effects and wake analyses has also been studied within the aircraft and turbo-machinery industries, using control volume analyses of energy/power, for instance by Denton (1993), Drela (2009) and Capitao Patrao et al. (2016). Designers developing novel aircraft concepts, such as Boundary Layer Ingestion (BLI), are actually dealing with very similar design challenges as ship propulsion system designers, with propulsion units operating in the wake of the craft, where the counteracting forces of thrust and drag cannot be studied separately.

Eslamdoost et al. (2017) applied a control volume analysis of energy on a self-propelled axisymmetric body to investigate the effect of propeller diameter variation on the system performance. However, to the authors knowledge, there are no other published studies where similar methodologies have been utilized for analyzing complete marine

* Corresponding author.
E-mail address: jennie.andersson@chalmers.se (J. Andersson).

https://doi.org/10.1016/j.oceaneng.2018.08.047
Received 13 March 2018; Received in revised form 17 August 2018; Accepted 24 August 2018

vessels with propulsion system.

The objective of this paper is to apply a methodology based on control volume analysis of energy for analyzing the ship propulsion interaction effects. The method will be exemplified on a model-scale 120 m single-screw cargo vessel to study the performance of an open and a ducted propeller in self-propulsion. The study is limited to one operating point, close to the design speed of the vessel.

2. Energy balance method

The methodology is based on evaluation of the energy equation over a control volume surrounding the propulsion system, with the flow field obtained through CFD. Control volume analyses, i.e. application of Reynolds Transport Theorem, is a well known tool within fluid mechanics. The specific application to marine propulsion units is described in Andersson et al. (2018) and Schuiling and van Terwisga (2016). Traditionally, the delivered power (P_D) is obtained from the propeller torque, i.e. forces on the propeller surface, and its rotation rate. However, by applying the energy balance method over a control volume enclosing the propulsion unit, P_D can also be obtained by integrating the energy fluxes and pressure work over the surfaces forming the control volume (CS),

$$P_D = \int_{CS} \left(\frac{p}{\rho} + \frac{1}{2}V_x^2 + \frac{1}{2}(V_t^2 + V_r^2) + \hat{u} + k \right)(\vec{V}\cdot\vec{n})dA + \dot{W}_{v,virtual}, \quad (1)$$

where $\vec{V}$ denotes the velocity vector, ρ density and $\vec{n}$ the normal vector to the control volume surface (positive outwards). Axial, tangential and radial velocity components are denoted by x, t and r, respectively. The energy flux is decomposed into kinetic energy in axial direction, kinetic energy in transverse directions, internal energy ($\hat{u}$) and turbulent kinetic energy (k). The axial direction is defined as the vessel sailing direction, i.e. not necessary identical to the propeller axis. There is also a contribution from pressure work (p) on the virtual (i.e. non-material) control volume surfaces. $\dot{W}_{v,virtual}$ is the work done by shear stresses on the virtual control volume surfaces, which often can be neglected, especially if the control volume surface is placed in regions without strong velocity gradients.

Fig. 1 illustrates the decomposed energy fluxes over a control volume surrounding the propeller and duct. Note that this is just a general representation, there will be inflow and/or outflow over all control volumes surfaces. Studying for instance the internal energy flux in Fig. 1: There will be a certain internal energy inflow to the control volume due to viscous dissipation occurring upstream the control volume, however the outflow of internal energy will exceed the inflow due to viscous dissipation within the control volume. The internal energy flux for this control volume will then constitute the difference between inflow and outflow. The sum of all energy fluxes over the control volume surfaces should match the delivered power to the propeller, evaluated based on forces on the propeller blades.

Decomposition of the delivered power into separate energy fluxes can be an aid for the designer to better understand and improve the performance of a system. This approach can also in the future be coupled with automated optimization procedures since it provides quantitative information on the hydrodynamic losses.

The analysis focuses on the performance within a certain control volume, implying that the control volume has to enclose the domain of interest. Possible options could be to enclose the entire vessel or only the aft ship. It is important to note that the control volume extension plays an important role in how one can distinguish and interpret the beneficial energy components from the unfavorable ones. For a control volume enclosing the entire vessel including the propulsion unit it is possible to distinguish the unfavorable energy components. This is more troublesome for a control volume only including a fraction of the hull, below we will elaborate on why. However, such a control volume can still be beneficial due to other reasons as will be discussed in Section 4.

Firstly, we discuss a control volume enclosing the entire vessel. In the ideal case, the propeller's slipstream would completely fill the wake behind the hull such that no axial kinetic energy flux is left behind the vessel. We also assume there will be no transverse kinetic energy flux over the control volume for an ideal vessel, and the viscous losses would be reduced to a minimum, i.e. zero (potential flow). Under these conditions it also holds that the rate of pressure work over the control volume would be zero. So, for an ideal vessel the sum of energy fluxes over the control volume would be zero, which implies zero delivered power to keep a constant speed forward. This idealization is naturally not practically possible, but it shows that for a control volume enclosing the entire vessel, all energy fluxes can be considered as unfavorable energy components, i.e. losses.

On the other hand, if the control volume only encloses a certain domain of the vessel, such as the aft ship, there needs to be an excess of useful energy flux over the control volume to be able to propel the remaining part of the hull at a constant speed. This implies that a fraction of the rate of pressure work and axial kinetic energy flux terms must be useful. In Andersson et al. (2018), the rate of pressure work and axial kinetic energy flux terms were decomposed into thrust power (useful) and axial non-uniformity loss. These axial non-uniformity losses are irreversible losses of pressure work and axial kinetic energy flux. They correspond to the total dissipation of pressure work and axial kinetic energy flux to internal energy that will occur downstream the control volume due to mixing out of spatial wake non-uniformity, i.e. the equalizing of pressure and velocity gradients to a homogeneous flow state. For a propeller operating in undisturbed inflow, the useful thrust power can be separated from the axial non-uniformity losses using either, an ideal control volume, or indirectly based on the forces

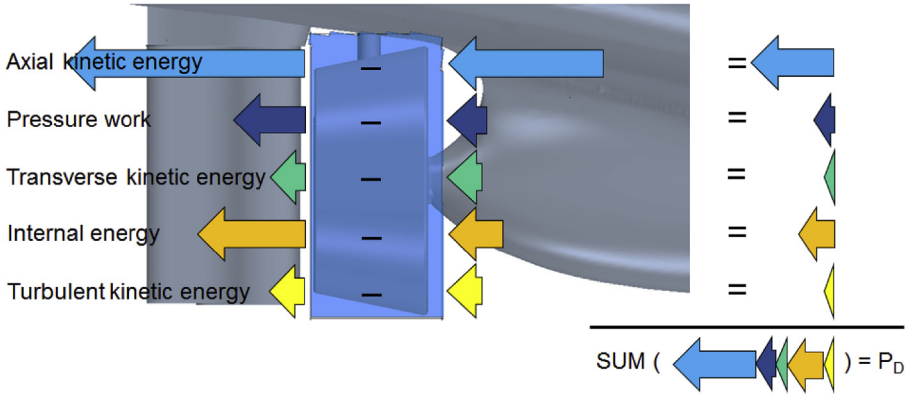

Fig. 1. General sketch of the decomposed energy fluxes over a control volume surrounding a ducted propeller operating behind a vessel. Note that this is just a general representation, there will be inflow and/or outflow over all control volumes surfaces.

on the propeller surface multiplied with the advance velocity. For an integrated system, such as a vessel with propulsion system, the decomposition into thrust power and axial non-uniformity losses is not possible due to unknown advance velocity.

The control volume analyses conducted in this study does not enclose a free surface. It is however possible to also include a free surface in the control volume. Compared to a double-body model the vessel resistance will be higher, for the control volume analyses it will imply more kinetic energy losses and viscous losses in the vicinity of the surface. This might be important if the propulsion system interacts with the free surface.

In the following sections the energy flux terms shown in Eq. (1) and their interpretation are presented in detail.

2.1. Pressure work and axial kinetic energy flux

Pressure work and axial kinetic energy fluxes originate from propulsor flow acceleration, as well as flow deceleration around the hull. As mentioned above, both these terms should be viewed as losses for a control volume enclosing the complete vessel, and for a control volume only enclosing a part of the vessel they constitute both useful thrust power and axial non-uniformity loss.

Considering again the ideal vessel, i.e. one where the propeller's slipstream completely fill the wake behind the hull. Independent of control volume, any deviation from this ideal condition should be viewed as loss, in this paper referred to as axial non-uniformity loss. Such a loss is caused by the mis-match between the propeller slipstream and hull wake, as well as flow non-uniformities within the propeller slipstream, which also is affected by the rudder. This implies that all velocity perturbations downstream the system, both positive and negative relative to the vessel speed, constitutes deviations from the optimal completely filled wake and indicates the presence of axial non-uniformity losses.

2.2. Transverse kinetic energy flux

Transverse kinetic energy flux is defined as kinetic energy flux in directions other than the vessel sailing direction. Transverse kinetic energy is often associated with radial and tangential velocity components induced by the propulsion unit, hull curvature or other reasons such as a propeller slipstream not being in line with the sailing direction. Transverse kinetic energy flux behind the vessel is considered as a loss, since the accelerated water in a direction else than the course of the vessel will not contribute to useful thrust. In case the transverse kinetic energy outflow of the control volume is reduced in comparison to that of the control volume inflow, this term will become negative which may indicate the recovery of the unfavorable transversal components to useful energy components.

2.3. Internal energy and turbulent kinetic energy flux

In a viscous flow, kinetic energy of the mean flow is converted to internal energy, i.e. heat, through two processes: (A) dissipation of turbulent velocity fluctuations, and (B) direct viscous dissipation from the mean flow to internal energy. Thus, the internal energy flux is a measure of both these processes, whereas the turbulent kinetic energy flux only accounts for an intermediate stage in (A). The turbulent kinetic energy has to be included only due to the CFD modeling, where turbulence is modeled using an eddy-viscosity model. All these energy fluxes should be rated as viscous losses, which are highly dependent on boundary layer losses and hence the velocity of the propeller blade relative to surrounding water, the size of wetted surfaces, and flow separation. Also the existence of spatial non-uniformities in the flow, such as circumferential variations associated with the finite number of blades, as well as flow structures like hub and tip vortices, contribute to increased viscous losses.

The internal energy is obtained through: $\hat{u} = c_p T$ (c_p = specific heat capacity, T = temperature), i.e. a temperature field is required from CFD, implying that the energy equation needs to be solved. Note that the temperature increase due to dissipation is very small, requiring well-resolved CFD results to obtain sufficient accuracy.

Before focusing on the analysis of the open and ducted propeller configuration using an energy balance analysis in Section 4, the details of the CFD-simulations will be outlined in Section 3.

3. CFD simulation of vessel in model scale

A model-sized (scale factor 1:22.629) single-screw 120 m cargo vessel with two alternative propulsion systems, an open and a ducted propeller, are in focus in this paper. These configurations have been studied in a previous research project at NTNU, Trondheim, and self-propulsion measurements of the same hull, both with open and ducted propeller, have therefore previously been carried out at MARINTEK (Bhattacharyya and Steen, 2014a; b). Rolls-Royce, as designers of the hull and open propeller, has a significant in-house knowledge about the open propeller configuration, and there may be possibilities for us to obtain full-scale performance data on this configuration in the future. In general, it is not recommended to study interaction effects between hull and propulsions system in model scale, because of a different wake field in comparison to the full scale. Moreover, since a tow force is applied to the model scale hull to compensate for the larger frictional resistance relative to full scale, the resistance and thrust are not in equilibrium. However, the main focus of this study is to apply and evaluate the energy balance methodology.

The full scale cargo vessel has a breadth of 20.8 m, a total displacement of 8832.7 m^3, a block coefficient of 0.657 and a nominal draught of 5.5 m. The aft-ship for the studied configurations, with open and ducted propeller, are shown in Fig. 2. Unfortunately, the detailed propeller geometry for the tested ducted propeller is not available for us, due to confidentiality. Therefore, based on available open water

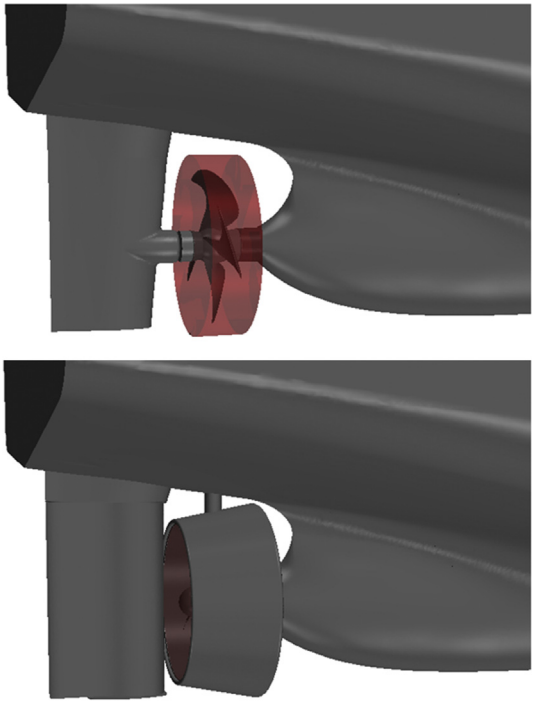

Fig. 2. Aft-ship geometry with open propeller (top) and ducted propeller (bottom) respectively. The region highlighted in red shows the propeller domain used for CFD-setup (see Section 3.1). (For interpretation of the references to colour in this figure legend, the reader is referred to the Web version of this article.)

Table 1
Characteristics of the model scale propellers.

	Open Propeller	Ducted Propeller
Number of blades	4	4
Propeller diameter (D_P)	185.6 mm	178.3 mm
Pitch ratio at r/R = 0.7	0.975	1.349
Blade area ratio	0.515	0.697
Rotation direction	Right handed	Right handed

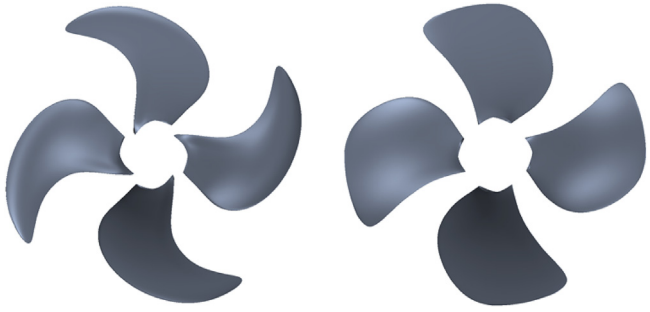

Fig. 3. Pressure side view from aft of open propeller (left) and ducted propeller (right).

characteristics, general characteristics of the propeller, and the detailed duct geometry, we have reconstructed a propeller for this study. The propeller characteristics for the open propeller and ducted propeller, as reconstructed, are provided in Table 1. The propellers are also depicted in Fig. 3. The section shape profiles for both propellers are similar to NACA16, the mean lines are close to NACA 0.8. The duct profile is a standard 19 A, with length equal to $0.54D_P$ (D_P = propeller diameter). The rudder designs are different for the two propulsion units (Bhattacharyya and Steen, 2014a; b). The open propeller is equipped with a Rolls-Royce Promas design, i.e. an integrated rudder bulb-propeller hubcap system, whereas the ducted propeller is not. The axial position of both propeller and rudder axis are identical for the two models.

Both systems are studied at Froude number = 0.203, corresponding to 1.449 m/s in model scale or 13.4 knots in full scale. To obtain comparable results for the two cases, the rotation rate of the propellers have been adjusted in CFD to meet the applied tow force in the model tests. Cavitation is expected to occur for both configurations, but the influence on performance is assumed negligible and is therefore not accounted for within this study.

For validation of the computations, the numerical simulations are carried out with a rotating propeller (sliding mesh) together with free water surface while the vessel is free to heave and pitch. However, due to slow convergence of the energy equation and limited computational resources, the energy balance analysis is performed on a model with the free surface modeled as a symmetry plane (double-body model), but still with a rotating propeller. Sinkage, trim and propeller rotation rate for the double-body model are taken from the corresponding free surface simulations results.

3.1. Computational domain

The size of the computational domain for the free surface simulations, given in [x, y, z] is [-3.5LPP:2.5LPP, -2LPP:2LPP, -1.5LPP:1LPP] ([0,0,0] located at mid-ship and LPP being the length between perpendiculars for the vessel). As stated earlier, the free surface is not modeled in the simulations used for the energy balance analysis and instead a horizontal plane at the undisturbed free surface level with symmetry boundary condition is used to determine the computational domains upper boundary. A separate domain for the propeller is constructed, as shown in Fig. 2. For the ducted propeller, the propeller region circumferential boundary consists of the inner surface of the duct.

The computational grids are generated using STAR-CCM + v10.06. The main domain consists of predominantly hexahedral cut-cells, created using the Trimmer mesher in STAR-CCM+. On hull and rudder, 7 prism layers along the material surfaces are applied. For the propeller domain, polyhedral cells, which are suitable for geometries with highly curved surfaces, are employed. Prism layers are extruded from the polyhedral surface mesh using the advancing layer mesher in STAR-CCM+. The boundary layers on propellers and duct are resolved using 15 prism layers near the walls with an expansion ratio of 1.3. A grid sensitivity study is not performed in this paper, however in order to ensure the mesh quality, the grids are constructed based on previous studies (Andersson et al., 2015) and (Andersson et al., 2018), which also discuss the influence of grid refinement on the energy balance analysis.

Wall functions are applied to model the boundary layers on the hull and rudder, since the available turbulence models in STAR-CCM + v10.06 provide a better resistance prediction with wall models. As shown in previous studies (Andersson et al., 2015), although the Reynolds Stress Model (RSM) predicts a more accurate wake field and resistance with resolved boundary layers, it is computationally expensive to use for free surface simulations due to that highly anisotropic cells, preferably used at the water surface, can result in convergence problems. The turbulence model k-ω SST with resolved boundary layers results in an under estimated hull resistance, which k-ω SST using wall functions does not suffer from, still the wake field may be less accurately resolved with the latter combination. However, our investigations shows that the computed bare hull wake field using k-ω SST with curvature correction together with wall functions is in a good agreement with the measured wake field for the hull used in this study. The propeller and duct boundary layers are resolved, by creating prism layers with $y^+ \approx 1$ and letting the code switch between wall functions and resolving the boundary layer down to the wall based on the local y^+ value.

Volumetric controls and anisotropic mesh refinements are used to refine the region close to the hull, the wake and the free surface. Except the region around the duct, identical mesh refinements are used for the case with open and ducted propellers. The region with refined grid at the stern is slightly larger for the double-body model compared to the free surface model. See Fig. 4 for the resulting mesh structure in the region surrounding the propeller and Table 2 for a summary of the number of cells. The average y^+ for the hull domain below the water surface is 60–80.

3.2. CFD simulation method

The commercial CFD package STAR-CCM + v10.06, a finite volume method solver, is employed. STAR-CCM+ is a general purpose CFD code used for a wide variety of applications. It solves the conservation equations for momentum, mass, energy, and turbulence quantities using a segregated solver based on the SIMPLE-algorithm. A second order upwind discretization scheme in space is used as well as a second order implicit scheme for time integration. In addition to the standard procedure for self-propulsion simulations, the energy equation is also solved. This enables the measurement of kinetic energy and turbulent kinetic energy dissipation in the form of a temperature rise in the flow.

First, the simulations are performed with free surface and the hull is free to heave and pitch together with a rotating propeller. The free surface is modeled using the Volume-of-fluid (VOF) method, implying that the domain consists of one fluid which properties vary according to the volume fraction of water/air. The convective term is discretized using the High Resolution Interface Capturing (HRIC) scheme. The heave and pitch motions are modeled with the Dynamic Fluid Body Interaction (DFBI) Equilibrium model in STAR-CCM+; the model moves the body stepwise to obtain balanced forces and moments

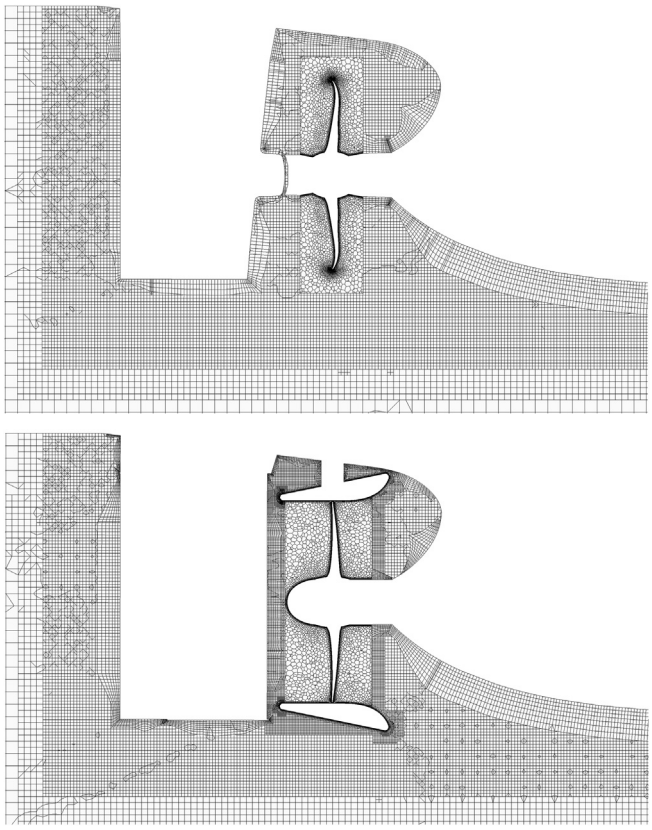

Fig. 4. Sectional cut at the symmetry plane of hull in aft-ship region for open (top) and ducted (bottom) propeller.

Table 2
Cell count for computational grids.

	Open Propeller	Ducted Propeller
Hull domain, free surface	$22.4{\cdot}10^6$	$28.7{\cdot}10^6$
Hull domain, double-body	$22.5{\cdot}10^6$	$28.8{\cdot}10^6$
Propeller domain	$8.6{\cdot}10^6$	$5.4{\cdot}10^6$

without solving the equations of motions. The propeller domain is rotating and sliding mesh interfaces have been applied between the domains.

An inlet velocity boundary condition of 1.449 m/s is specified at the inlet and lateral boundaries. On the outlet, a hydrostatic pressure is prescribed for the free surface setup and a uniform static pressure for the double-body model. The water surface level is initialized as the declared draft of the hull. Turbulence is modeled using k-ω SST with curvature correction, as discussed in Section 3.1.

In the beginning, to speed up the simulation procedure, the cases are run with a larger time step and a fixed propeller, utilizing Multiple Reference Frames (MRF) to simulate propeller rotation with frozen rotor interfaces. The hull is released to freely heave and pitch after the forces are stabilized. Thereafter, when sinkage, trim and hull resistance again are stabilized the time step is reduced to a value corresponding to 1° propeller rotation per time step. When overall results are stabilized after time step reduction, the propeller domain is set to rotate using sliding mesh. The rotation rate of the propeller is adjusted to meet the applied tow force from model tests. This is performed manually since the simulation is very slow in reacting to changes in rotation rate, and not much time would have been gained by automation. The simulations are run until the initial transients have disappeared, typically occurring after 20–100 propeller revolutions. Thereafter they are run for further five revolutions before data is gathered.

Table 3
Results for self-propulsion validation, difference to measured data presented within brackets. For the ducted propeller, K_T represents the total thrust from propeller and duct.

	Open Propeller		Ducted Propeller	
	Test	CFD	Test	CFD
Tow force [N]	9.37	9.11 (-2.8%)	9.37	8.94 (-4.5%)
Rotation rate, n [rps]	8.872	8.83 (-0.5%)	7.696	8.00 (4.0%)
K_T	0.2065	0.193 (-6.7%)	0.337	0.314 (-6.8%)
K_{TD}	–	–	0.0589	0.0092 (-84%)
K_Q	0.0345	0.0316 (-8.4%)	0.0645	0.0669 (3.8%)
η_0	0.591	0.595 (0.6%)	0.604	0.549 (-9.2%)

Finally, the double-body simulations are performed, with trim, sinkage and propeller rotation rate obtained from the free surface simulation results. These simulations are also initialized using MRF and thereafter applying sliding mesh interfaces with a time step corresponding to 1° propeller rotation.

3.3. Validation

CFD results are compared to test data (Bhattacharyya and Steen, 2014a; b) in Table 3. The propeller open water efficiencies $\eta_0 (= thrust{\cdot}V_A/P_D)$ have been obtained through thrust-identity, using open water performance data from corresponding open water CFD-results (not described within this article, but propeller domain identical to the one used for self-propulsion). For the ducted propeller, K_T represents the total thrust from propeller and duct.

As mentioned earlier, the propeller rotation rate has been adjusted to match the tow force used in the towing tank tests. This adjustment is an iterative procedure and for computationally expensive simulations it becomes very time consuming to find the exact rotation speed which corresponds to the applied tow force. As a result, the tow force used in the simulations turned out to be 2.8 and 4.5% lower than the corresponding towing tank values for the open and ducted propeller, respectively. This also implies that the simulated tow force is 1.8% lower for the ducted propeller compared to the open propeller.

The comparison with tests, as shown in Table 3, is not very impressive for any of the configurations. For both cases the thrust predicted by CFD is low compared to test data, despite that the tow force is lower than test for both cases, which theoretically should mean higher loaded propellers. This ought to mean that either the thrust deduction or hull resistance is under-estimated. The CFD predicted bare hull resistance differed only -0.9% compared to commercial model tests conducted using the same model, but at another occasion (test data being Rolls-Royce IP and therefore not possible to disclose). Within that test campaign, also the bare hull wake field was measured, and the agreement between CFD and these measurements is considered relatively good. However, even if both thrust coefficient K_T $(= thrust/(\rho n^2 D_P^4))$ and torque coefficient K_Q $(= torque/(\rho n^2 D_P^5))$ are inaccurately predicted, the open propeller efficiency is actually relatively well predicted by CFD in self-propulsion. This is unfortunately not the case for the ducted propeller configuration. As mentioned earlier, a complicating matter is that the ducted propeller geometry in the CFD setup is not identical with the one tested. The CFD-method used for the ducted propeller in open water has previously been validated (with good results) and K_{TP} (propeller thrust coefficient) and K_Q for the reconstructed propeller were both in good agreement with available open water results (~ +1%). However, just as in self-propulsion the duct thrust was clearly under-predicted in open water. The duct exhibits a distinct separation behind the leading edge in both operating conditions. It is a well-known fact that k-ω SST has a tendency to over predict separations, which may be the case here. Now, with some perspective on the study, alternatives to, or modifications of the k-ω SST turbulence model with curvature

correction should have been considered in an earlier phase of the project to better predict the duct separation. We should neither neglect that the propeller-duct interaction may be poorly captured due to differences in simulated and tested propeller geometry, which also may influence the duct thrust. CFD also overestimate the ducted propeller torque, which may be associated to the deviation in propeller rotation rate from the measured value by 4%, which in turn can be a consequence of the tow force mismatch.

This validation exercise shows that the CFD-results, especially for the ducted propeller configuration, is not fully representative for the tested conditions. The energy balance analysis conducted in Section 4 could therefore only be claimed to be valid for the computed setups.

Further, since accurate CFD results are crucial for the outcome of an energy balance analysis, more effort needs to be spent on obtaining accurate CFD methods representative for model as well as full scale conditions. Due to that the detailed test conditions and procedures, beside the exact geometry, are unfamiliar to the authors for this case, there may be a risk that the computed and tested configurations differ more than what we are aware of. The test case is thus not optimal for a fair comparison of the two configurations, but is still deemed satisfactory to use for demonstrating the principles and application of an energy balance analysis on two different propulsion system configurations.

To justify the use of a double-body model for the energy balance analysis, K_T, K_{TD}, and K_Q are compared to the free surface model results in Table 4. The relative differences are negligible in comparison to the correspondence between test data and CFD. Possible reasons behind the deviations are influences from the free surface not accounted for in the double body model, improper convergence of free surface simulations or the grid differences between free surface and double-body model setups.

4. Energy balance analysis of vessel in model scale

The energy balance analysis is applied on the vessel with open and ducted propeller. First, the energy balance over three different control volumes enclosing the propeller, the aft-ship and the entire vessel, are evaluated and discussed in Section 4.1. Then, in Section 4.2, for a more detailed evaluation of the performance of each case, the aft-ship control volume is applied.

The control volumes are established as a post-processing step, using ”derived parts” in STAR-CCM+. The control volume boundaries are all located within the outer domain, which has a cut-cell grid aligned with a Cartesian coordinate system. To minimize interpolation errors, the shape of the control volumes in this study is therefore a rectangular box, aligned with the same coordinate system as the grid.

Since we are dealing with a transient flow, the energy fluxes through the control volume should be averaged over a certain time interval to accurately represent conversion of propeller shaft power to different energy components. However, a simplification has been carried out within this study and the presented results are obtained through averaging of three different propeller positions, with the reference blade located at 0° (defined as the top position), 30° and 60°. In this paper, all graphic visualization of the results will be taken with the reference blade position at 60°.

Table 4
Difference in K_T and K_Q between free surface and double-body model simulation results. For the ducted propeller, K_T represents the total thrust from propeller and duct.

	Open Propeller		Ducted Propeller	
	Free surface	Double-body	Free surface	Double-body
K_T	0.193	0.195 (1.0%)	0.314	0.321 (2.2%)
K_{TD}	–	–	0.0092	0.0130 (41%)
K_Q	0.0316	0.0320 (1.4%)	0.0669	0.0675 (0.8%)

Fig. 5. Alternative control volumes. A) Enclosing the propeller, B) enclosing the aft-ship and C) enclosing the entire vessel.

Throughout the analyses, the work performed by shear stresses on the imaginary control volume surface is not included, since it constitutes less than 0.01% of the total energy balance for the applied control volumes.

Note that all energy balances are influenced by the fact that the systems are not in force equilibrium, due to the applied tow force for compensation of scale effects. This study is limited to analysis of the systems in model scale, results which cannot be directly transferred to full scale.

4.1. Establishment of control volume

Establishment of a suitable control volume is a critical stage of the system energy balance investigation. Three different control volumes are here discussed and suggested, enclosing the propeller (A), the aft-ship (B) and the entire vessel (C), all illustrated in Fig. 5. The extensions of the control volumes are identical for the open and ducted propeller cases which are within the refined grid regions surrounding the vessel. The energy balance for each of these control volumes is specified in Tables 5 and 6, for the open and ducted propeller configuration, respectively. All numbers included in the tables are round off presentation of the computed values, therefore the sum may not match the individual components exactly. To better illustrate the difference between the control volumes the energy balance analysis for the open propeller is also shown as a bar chart in Fig. 6.

The discrepancy between delivered power, evaluated based on forces acting on the propeller, and control volume energy balance varies within the range of -0.7–2.9%. Considering that the propeller is operating in an inhomogeneous wake behind the vessel and the transient flow in the vicinity of the propeller, the agreement is reasonable. Among the studied control volumes the agreement is poorest for the control volume enclosing the aft-ship (B), which may be associated with large flow fluctuations on control volume boundaries in this region not directly linked to propeller load variations. Moreover, the effect of numerical dissipation, numerical convergence and inaccuracies of evaluating energy fluxes over the control volume surface could also be contributing to the reported discrepancy.

The energy balance for control volume A represents the flow field

Table 5
Energy balance for open propeller configuration.

Control volume	A	B	C
Pressure work	11.11 (36%)	18.54 (59%)	47.90 (159%)
Axial kinetic energy flux	11.83 (38%)	3.36 (11%)	−56.19 (-186%)
Transv. Kinetic energy flux	1.23 (4.0%)	−0.46 (-1.5%)	2.42 (8.0%)
Internal energy flux	6.45 (21%)	9.64 (31%)	35.28 (117%)
Turb. Kinetic energy flux	0.12 (0.4%)	0.22 (0.7%)	0.77 (2.6%)
Sum energy balance	30.75	31.30	30.19
Propeller power, P_D	30.54	30.54	30.54
Difference	*−0.7%*	*2.5%*	*−1.1%*

Table 6
Energy balance for ducted propeller configuration.

Control volume	A	B	C
Pressure work	6.11 (16%)	18.48 (46%)	46.31 (118%)
Axial kinetic energy flux	23.24 (59%)	6.24 (16%)	−52.58 (-134%)
Transv. Kinetic energy flux	0.81 (2.0%)	0.05 (0.1%)	3.11 (7.9%)
Internal energy flux	8.90 (23%)	14.91 (37%)	41.20 (105%)
Turb. Kinetic energy flux	0.30 (0.8%)	0.54 (1.4%)	1.09 (2.8%)
Sum energy balance	39.35	40.23	39.14
Propeller power, P_D	39.10	39.10	39.10
Difference	*0.6%*	*2.9%*	*0.1%*

over the propeller. The axial kinetic energy flux and pressure work terms are a direct consequence of the propeller thrust generation; a pressure difference is produced between the forward and rear surfaces of the blade and the water is accelerated downstream. As described in Section 2, a fraction of these terms will however be axial non-uniformity losses due to for instance the circumferential variations associated with the finite number of blades and tip vortices. For a propeller in undisturbed inflow the decomposition into useful thrust power and axial non-uniformity losses can be performed indirectly through evaluation of the thrust power based on forces acting on the propeller blades multiplied with the advance velocity. This cannot be conducted with similar accuracy for a propeller operating in behind due to undefined advance velocity. The transverse kinetic energy flux component mainly represents the deflection of the flow over the propeller blades, and hence is positive for both configurations. The internal energy and turbulent kinetic energy flux describes the viscous losses over the propulsion unit, which to the largest extent is due to boundary layer losses, but also can incorporate the mixing out of velocity gradients within the flow, such as the tip vortices. Since control volume A describes the flow in the vicinity of the propeller, it is suitable for isolated studies of the propeller hydrodynamics but it cannot capture the interaction effects between the hull, propeller and rudder. Therefore, this control volume is less suitable for analyzing the system performance.

In order to resolve the aforementioned limitations of control volume A, control volume B is proposed. This control volume encloses a larger extent of the aft ship as well as the propulsor and the rudder. The inflow to this control volume constitutes of hull boundary layer. The positive pressure work and axial kinetic energy flux terms (Fig. 6) are associated with a net positive thrust power over the material boundaries enclosing the control volume. For a vessel at constant speed the net thrust within the control volume should balance the net drag on the remaining part of the hull outside the control volume minus the tow force. Similar to control volume A, the pressure work and axial kinetic energy flux terms also constitutes of an axial non-uniformity loss, and neither for this control volume is it easily quantified, since an advance velocity cannot be defined. However, through an understanding of the origin of the axial non-uniformity loss, i.e. non-uniformities in the flow, other qualitative methods can be applied. Concerning the transverse kinetic energy flux, control volume B incorporates possible bilge vortices, the propeller slipstream rotation as well as rudder performance since it extends sufficiently far upstream and downstream of the aforementioned regions. The transverse kinetic energy flux term obtained for control volume B has a minor contribution to the total energy balance for both of the open and ducted propeller configurations. This small contribution is caused by a transverse inflow through the lateral boundaries due to propeller suction which is canceled out by the propeller slipstream which to various extent is straightened up over the rudder. The internal and turbulent kinetic energy fluxes describes all viscous losses occurring within the control volume.

An alternative solution to avoid the net positive thrust power of unknown magnitude, present for both control volume A and B, to facilitate the quantification of the axial non-uniformity losses, is to apply a larger control volume which encloses the entire vessel. With such a large control volume the entire vessel is in focus, not only the propulsor or aft-ship. The negative axial kinetic energy flux is caused by the fact that the vessel slows down the surrounding water more than accelerating it. The magnitude of the axial kinetic energy flux term is smaller for the ducted propeller configuration, due to larger flow acceleration over the propulsion unit and hence smaller axial kinetic energy flux deficit in the vessel wake. The pressure work term is positive which, considering the negative axial kinetic energy flux and Bernoulli's principle, is relatively intuitive to argue. The transverse kinetic energy flux is mainly a combination of an inflow to the control volume from its lower side due to propeller suction and an outflow exceeding this downstream the rudder within the propeller slipstream. The internal and turbulent kinetic energy fluxes are much larger in comparison to control volume A and B, since boundary layer losses for the entire vessel are included. The differences between the compared propeller configurations to a large extent originate from the aft-ship since the remaining parts are identical. As described in Section 2, for an ideal self-propelled system using a control volume surrounding the entire vessel, the energy

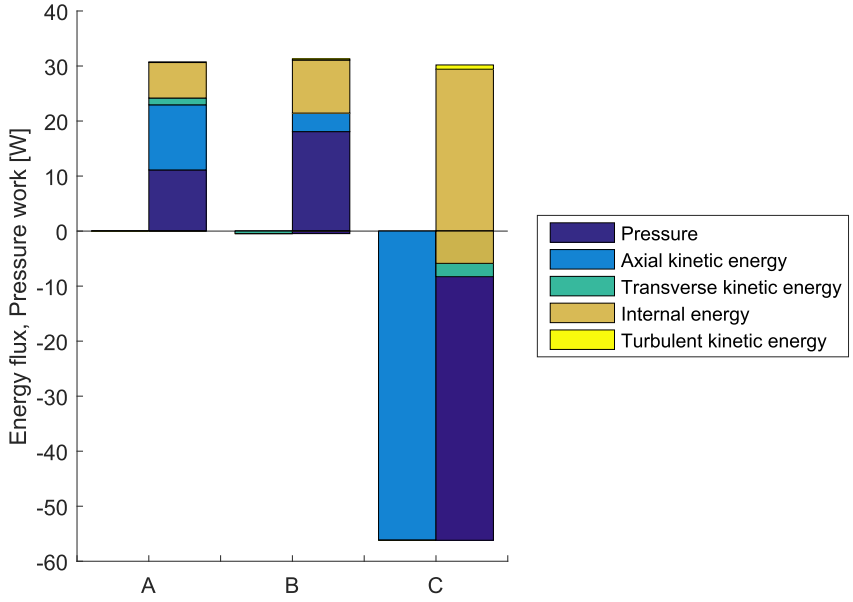

Fig. 6. Energy balance for open propeller configuration using control volume A, B and C, respectively (detailed data available in Table 5).

balance should sum up to zero. This implies that the combined axial kinetic energy flux and pressure work term ideally should be zero. For the studied cases the aforementioned sum results in negative values, -8.29 W and -6.26 W, for the open and ducted propeller respectively. Intuitively, these negative values can be interpreted as a higher performance compared to the theoretically optimal one. However, we should not forget the existence of an external tow force acting on the system. The assisting unloading power of the tow force can be expressed by multiplying the tow force with the ship speed, -10.46 W. However, due to axial non-uniformity losses the sum of the axial kinetic energy flux and pressure work terms does not sum up to the unloading tow force power. The difference between these values represent the axial non-uniformity losses seen from the perspective of control volume C, which are 2.18 W and 4.20 W for the open and ducted propellers, respectively.

We believe that the most complete picture of the system is obtained through control volume C enclosing the complete vessel. Using this control volume, even weaker effects such as increased boundary layer losses far upstream due to an altered propeller suction are captured, and it is possible to quantify the axial non-uniformity loss. The energy balance is however more difficult to grasp and use for pedagogical explanations, especially since the axial kinetic energy flux and pressure work consists of positive and negative contributions from wake and propulsor slipstream that cancel each other. Control volume A cannot be used to capture the interaction effects between stern, propulsor and rudder. Thus control volume B in this study is considered to be the most practical configuration for analyzing the system performance and will be used for comparison of the open and ducted propeller in Section 4.2.

4.2. Analysis of open and ducted propeller configurations using an energy balance

As shown in Tables 5 and 6 the total required delivered power is increased by 28% for the ducted propeller configuration compared to the open propeller, according to the CFD-results. The difference in open water efficiencies computed by CFD, as listed in Table 3, is much less than this observed difference in delivered power. Note also that the sinkage and trim for the respective configurations are almost the same, -7.1/-6.8 mm and 0.067/0.071°, and thus not expected to contribute significantly to the difference in delivered power. Using the energy balance analysis, we will try to examine the reasons behind the power discrepancy. Note also that this complete discussion will focus on the flow conditions as computed by CFD, which disfavor the ducted propeller configuration in relation to tested cases, see Section 3.3. But in general, a shorter duct is most often favored at operating points similar to the studied one and modern duct profiles with better performance at such speeds are available.

The energy balance analysis for the open and ducted propeller configurations using the control volume enclosing the aft-ship (B) is illustrated in Fig. 7. The internal energy flux is 55% higher for the ducted propeller configuration, which is an indication of much higher viscous losses. The transverse kinetic energy flux is negative for the open propeller configuration and positive for the ducted propeller. This implies a gain of transverse kinetic energy flux for the open propeller, seen from the perspective of control volume B, however the overall contribution to the total energy balance from this term is quite small. The combined axial kinetic energy flux and pressure work terms are 13% higher for the ducted propeller configuration. The useful thrust power for the ducted propeller configuration is most probably not very much different from the open propeller to propel the remaining part of the hull outside the control volume, thus the axial non-uniformity loss is most probably higher for the ducted propeller configuration to cover the difference, which also was indicated using control volume C in Section 4.1.

An attempt is made to explain important factors contributing to the system performance through separation of the energy balance over control volume B into three internal control volumes, upstream the propeller, over the propeller, and over the rudder, as illustrated in Fig. 8. This data is provided in Tables 7 and 8. Since internal energy is a measure of dissipation of kinetic energy into heat, the turbulent kinetic energy, which is an intermediate stage in this process, is not included within this analysis. Further, since the transverse kinetic energy component is minor for both cases and relatively straightforward to analyze, less attention is paid to this component in the discussion below.

A constant vessel speed is assured when the useful thrust matches the resistance of the entire vessel with a working propulsion unit. The analysis is complex since thrust and resistance are tightly coupled, i.e. an increased resistance implies a higher thrust. A higher thrust is associated with higher velocities through the propulsion unit and thus increased viscous losses as well as an impaired pressure recovery on the hull upstream the propeller and increased forces on the rudder, i.e. an even higher resistance. Tables 7 and 8 show that more pressure work/axial kinetic energy is generated over the ducted propeller, 5.5 + 23.8 W, compared to 12.3 + 10.7 W over the open propeller, i.e. a larger acceleration of the flow over the propulsor. The thrust coefficients as listed in Table 3 also correspond to a higher thrust for the ducted propeller case, 20.3 N compared to 17.8 N.

Furthermore, it can be observed that the dissipation of kinetic energy to internal energy is higher for the ducted propeller configuration, both over the propeller (+38%) and over the rudder (+143%), while the differences over the upstream part are much smaller. This increased internal energy flux is caused by a set of reasons, such as increased boundary layers losses due to higher induced velocities and larger wetted surfaces, and mixing out of spatial wake non-uniformities. The minor increase over the upstream part is the easiest one to understand; it can only be caused by increased boundary layers losses due to higher induced velocities by the propulsion unit, since the geometry within this control volume is identical for both configurations.

The internal energy flux through the interface between the propeller and rudder control volumes are depicted in Fig. 9. For the ducted propeller configuration, it is clear that the duct contributes to a large share of the increased viscous losses. Amplified levels of internal energy flux are noticed on both outer and inner side of the duct. The semi-circular form of high internal energy flux surrounding the duct originates from the flow separation behind the duct leading edge. On the inner side, the viscous losses to a large extent steam from the propeller tip-vortex/duct interaction. For both configurations higher internal energy fluxes are observed in the right hand side blade wakes, which are a consequence of more heavily loaded blades in the wake peak. To reduce the internal energy flux, i.e. the viscous losses, for the ducted propeller, a shorter duct would of course be beneficial, implying less boundary layer losses, also a propeller-duct interaction implying less viscous losses, as well as a duct with less tendency to separation. For both cases, a less pronounced wake peak would reduce the viscous losses.

A large difference in performance is observed over the rudder. The energy balance in Tables 7 and 8 shows that the overall energy conversion process is from pressure work and transverse kinetic energy to axial kinetic energy and internal energy for both configurations. However, for the open propeller, 6.5 W is converted to axial kinetic energy, while the figure for the ducted propeller configuration is only 0.9 W, with a much larger share of conversion to internal energy flux (+143%), i.e. energy disappearing into viscous losses.

The internal energy flux behind the rudder is depicted in Fig. 10. For the open propeller it is clear that the internal energy fluxes at this instance deduce from the blade boundary layer losses and mixing out of tip-vortices, as well as from the rudder boundary layer losses. The levels are higher on the right hand side of the rudder, which is due to the higher losses originating from the propeller slipstream at this location, but also enhanced by the rudder boundary layer losses which are larger on the ”rudder suction side”, i.e. the upper right and lower left sides of the rudder. The internal energy flux for the ducted propeller at this

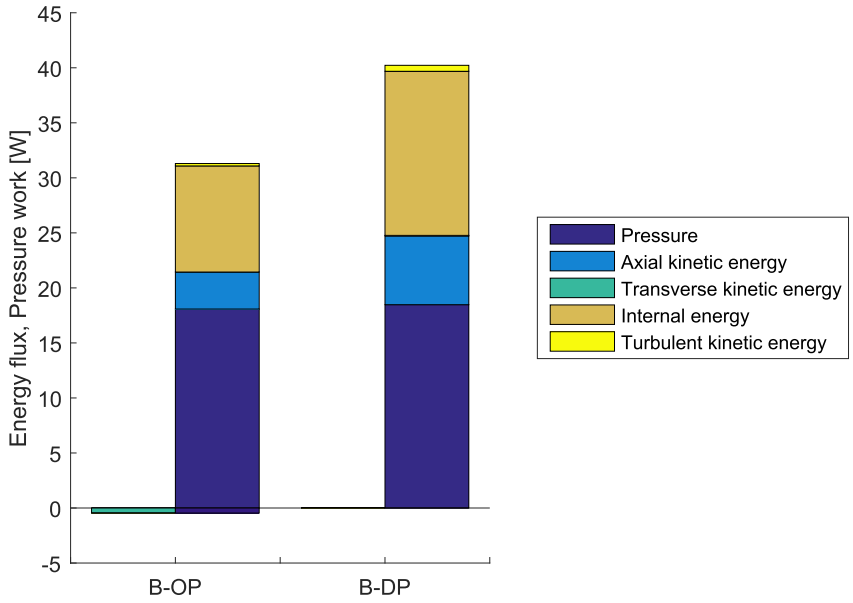

Fig. 7. Energy balance for open and ducted propeller configurations using control volume B (detailed data available in Tables 5 and 6).

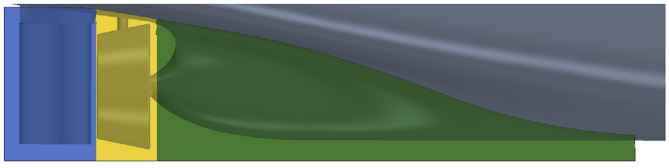

Fig. 8. Control volumes B separated into three internal control volumes; upstream the propeller, propeller and rudder.

Table 7
Energy balance for open propeller configuration, applying control volume B separated according to Fig. 8.

	Rudder	Propeller	Upstream	Total
Pressure work [W]	−6.0	12.3	12.3	18.5
Axial kinetic energy flux [W]	6.5	10.7	−13.9	3.4
Transv. Kinetic energy flux [W]	−2.2	1.0	0.7	−0.5
Internal energy flux [W]	1.9	6.4	1.3	9.6

Table 8
Energy balance for ducted propeller configuration, applying control volume B separated according to Fig. 8.

	Rudder	Propeller	Upstream	Total
Pressure work [W]	−2.6	5.5	15.6	18.5
Axial kinetic energy flux [W]	0.9	23.8	−18.5	6.2
Transv. Kinetic energy flux [W]	−2.7	0.9	1.8	0.05
Internal energy flux [W]	4.6	8.9	1.4	14.9

plane is more irregular, and can be traced back to several flow features. Firstly, from the propulsion unit we have both the duct and propeller losses, in addition to that the different rudder design seems to contribute significantly to the higher internal energy flux. For the ducted propeller case, the hub vortex hits the rudder leading edge due to the lack of a rudder bulb and hub cap, the rudder profile is also thicker (+25%) and less streamlined. Moreover, the rudder for the ducted propeller configuration has oval-shaped horizontal plates on the upper and lower edges, from which the internal energy flux traces are clearly visible in Fig. 10. Since the propeller slipstream accelerates to higher velocities for the ducted propeller configuration, higher boundary layer losses are expected. To be able to quantify the additional losses associated with the different rudder designs, it could have been of interest to study them separately in otherwise identical configurations. In general, to improve the systems through enhancing the rudder hydrodynamic performance, the viscous loss associated with the rudder is one important parameter, which is easily visualized through the internal energy flux. However, the viscous losses must be studied together with the other energy fluxes (as well as maneuvering capacity), since a reduction in the viscous losses may imply an increase in any of the other energy components.

To get further insight in the usefulness of the axial kinetic energy flux/pressure work term, these terms can also be visualized. In general, large velocity (or pressure) perturbations relative to the vessel speed imply strong gradients in the flow field that eventually will mix out downstream and dissipate in the form of internal energy. In other words, to minimize the axial non-uniformity losses, as homogeneous flow field as possible is preferable. Figs. 11 and 12 show the axial kinetic energy flux through sections located between the propeller and the rudder as well as downstream the rudder, respectively. A less uniform wake is noted for the ducted propeller configuration at both instances, which implies higher axial non-uniformity losses, since these flow fields will need to equalize downstream. This also means that the spatially non-uniform ducted propeller slip stream, depicted in Fig. 11, most probably contribute to the large conversion to internal energy over the rudder region as noted above.

The level of axial flow non-uniformity can possibly be evaluated through analyzing the conversion to internal energy flux over a control volume downstream the rudder. However, difficulties arise when the region with reasonably refined grid behind the vessel is too short so the rate of conversion to internal energy has the same order of magnitude as the accuracy of the energy balance method in an unsteady flow, as observed in this study.

Some possible use of the energy balance analysis for design improvements have been brought up above. However, on a more general level, from the energy balance perspective there are three overall strategies to improve the system: reducing transverse flows behind the vessel; obtaining a more uniform flow field in the axial direction; and reducing viscous losses. An improvement in one aspect often implies an increment in other losses, for instance a reduction in transverse kinetic losses often costs in form of increased viscous losses. To be able to predict the interplay between the various loss components in advance, experience of the use of energy balance analyses is preferable. To facilitate learning between projects, a standardized methodology for both

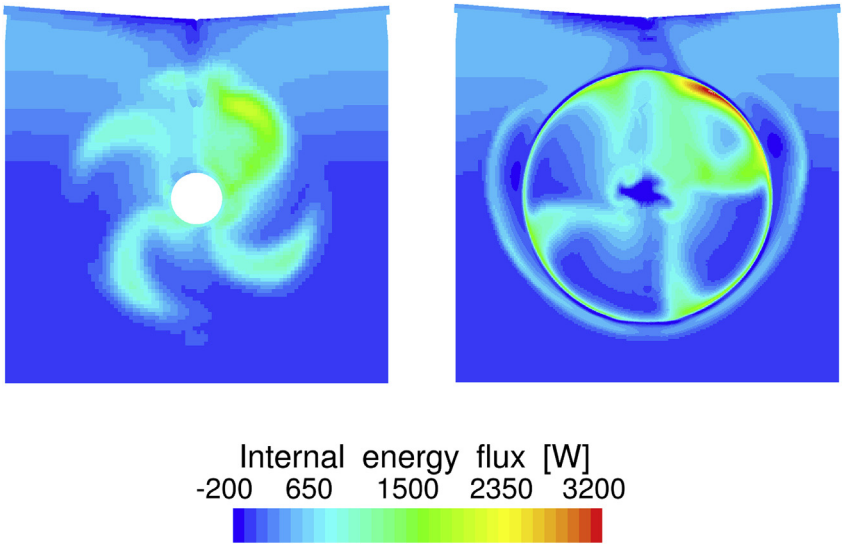

Fig. 9. Contour plot of internal energy flux at interface between propeller and rudder control volumes. Open propeller (left) and ducted propeller configuration (right).

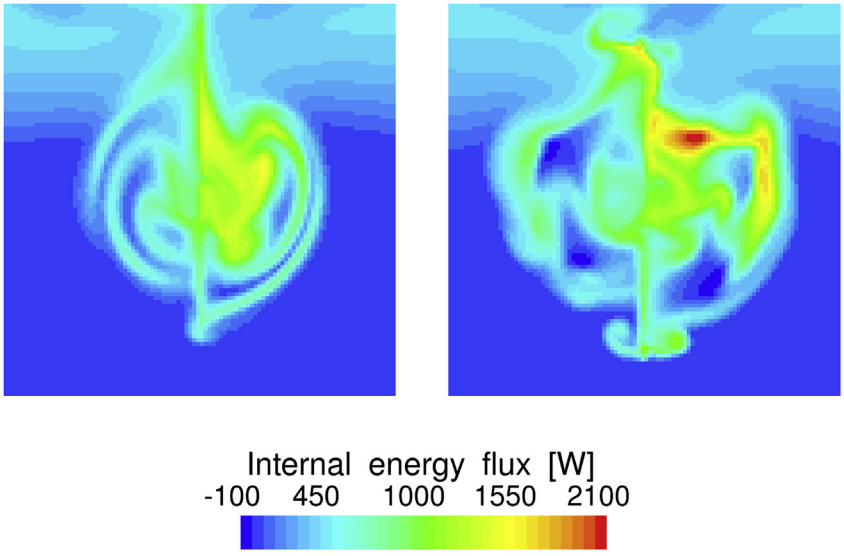

Fig. 10. Contour plot of internal energy flux at control volume B downstream boundary (behind rudder). Open propeller (left) and ducted propeller configuration (right).

CFD-setup and post-processing is highly recommended, since the distribution into the various energy flux components is depends not only on control volume extension, but also computational grid.

5. Conclusions

We have shown that a control volume analysis of energy applied on CFD results provide an alternative approach for studying the required delivered power of a vessel. The energy balance analysis is not a method replacing the traditional propulsive factors for ship-scale performance predictions, but however a promising tool for describing, understanding, and improving flow physics and associated system performance, independent of system configuration. It is a post-processing tool with the only additional requirement of solving the energy equation, which can be employed in any CFD-code based on commonly available variables.

The energy balance analysis provide a very good illustration of the viscous losses, through internal and turbulent kinetic energy fluxes, as well as transverse kinetic energy losses. The axial non-uniformity losses are mostly illustrated visually in this paper. However, similar to the other loss components, the quantification of the axial non-uniformity losses is of a great interest and will be studied in the future. Associated with this is also studies on the most suitable control volume for these kind of analyses for a range of configurations. Additionally, further understanding of the required power can be achieved by studying the flow field and energy balance through out a full blade revolution cycle.

The method is fully dependent on CFD-results to describe the flow around the vessel and propulsion unit accurately. Therefore further method validation has to be carried out for different types of vessels and propulsor configurations at various operating conditions, in both model and full scale.

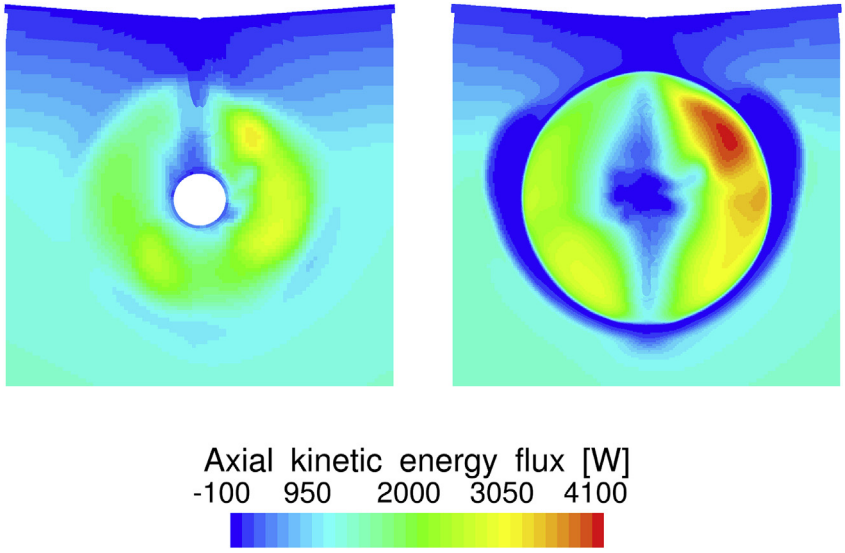

Fig. 11. Contour plot of axial kinetic energy flux at interface between propeller and rudder internal control volumes. Open propeller (left) and ducted propeller configuration (right).

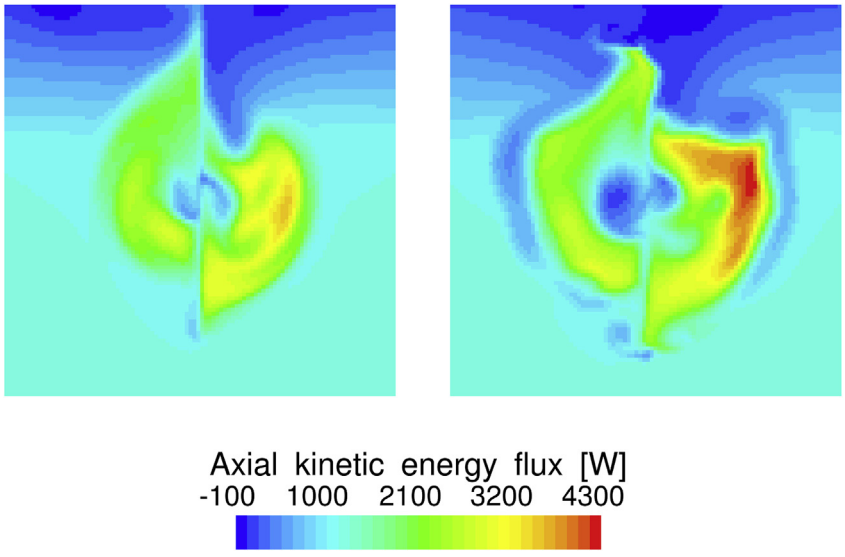

Fig. 12. Contour plot of axial kinetic energy flux at control volume B downstream boundary (behind rudder). Open propeller (left) and ducted propeller configuration (right).

Acknowledgements

This research is supported by the Swedish Energy Agency (grant number 38849-1) and Rolls-Royce Marine through the University Technology Centre in Computational Hydrodynamics hosted by the Department of Mechanics and Maritime Sciences at Chalmers. The simulations were performed on resources at Chalmers Centre for Computational Science and Engineering (C3SE) provided by the Swedish National Infrastructure for Computing (SNIC).

References

Andersson, J., Eslamdoost, A., Capitao-Patrao, A., Hyensjö, M., Bensow, R.E., 2018. Energy balance analysis of a propeller in open water. Ocean Eng. 158, 162–170.

Andersson, J., Hyensjö, M., Eslamdoost, A., Bensow, R., 2015. CFD simulations of the Japan bulk Carrier test case. In: Proceedings of the 18th Numerical Towing Tank Symposium. Cortona, Italy.

Bhattacharyya, A., Steen, S., 2014a. Influence of ducted propeller on seakeeping in waves. Ocean Eng. 91, 243–251.

Bhattacharyya, A., Steen, S., 2014b. Propulsive factors in waves : a comparative experimental study for an open and a ducted propeller. Ocean Eng. 91, 263–272.

Capitao Patrao, A., Avellán, R., Lundbladh, A., Grönstedt, T., 2016. Wake and loss analysis for a double bladed swept propeller. In: Proceedings of ASME Turbo Expo 2016. Seoul, South Korea.

Denton, J.D., 1993. The 1993 IGTI scholar lecture loss mechanisms in turbomachines. J. Turbomach. 115, 621–656.

Drela, M., 2009. Power balance in aerodynamic flows. AIAA 47 (7), 1761–1771.

Eslamdoost, A., Andersson, J., Bensow, R., Gustafsson, R., Hyensjö, M., 2017. Analysis of propeller-hull interaction phenomena on a self-propelled axisymmetric body. In: Proceedings of the Fifth International Symposium on Marine Propulsors. Espoo, Finland.

Schuiling, B., van Terwisga, T., 2016. Energy analysis of a propeller in open water using a RANS method. In: 24th International HISWA Symposium on Yacht Design and Yacht Construction. Amsterdam, The Netherlands.

van Terwisga, T., 2013. On the working principles of energy saving devices. In: Proceedings of the Third International Symposium on Marine Propulsors. Launceston, Tasmania, Austrailia.